Asian Journal of Chemistry; Vol. 34, No. 4 (2022), 917-925

ASIAN JOURNAL OF CHEMISTRY

https://doi.org/10.14233/ajchem.2022.23516

A Ruthenium(II) Nitrosyl Complex of *N*-Dehydroacetic Acid-Sulfadiazine: Synthesis, DFT Studies and *in silico* ADME Properties

P.S. JAGET, P.K. VISHWAKARMA*, M.K. PARTE and R.C. MAURYA

Department of P.G. Studies and Research in Chemistry and Pharmacy, Rani Durgavati Vishwavidyalaya, Jabalpur-482001, India

*Corresponding author: E-mail: inorgpkv85@gmail.com

Received: 5 September 2021; *Accepted*: 3 January 2022; *Published online*: 10 March 2022; AJC-20734

A sulpha drug-derived Schiff base ligand *N*-dehydroacetic acid-sulfadiazine was synthesized by treatment of dehydroacetic acid and sulfadiazine. A mononuclear Ru(II) nitrosyl complex of the Schiff base ligand *cis*-[$RuCl_2(NO)(PPh_3)$(dha-sdz)] was synthesized. The complex was characterized by spectral (IR, ^{1}H NMR and UV/visible) techniques and physico-chemical studies. A cyclic voltammetric technique observed the electrochemistry of the complex compound. Therefore, the Gaussian 09 programme has been used to optimized molecular structure, electronic surface analysis, NLO properties through DFT approaches *via* mixed basis set at B3LYP/LANL2DZ level of theory. The ^{1}H NMR spectrum of complex compound was computed with the GIAO method and correlated to experimental chemical shift. The TD-DFT based electronic absorption spectrum was computed using the PCM model. Additionally, the synthesized compound was predicting its *in silico* ADME properties, showing good physico-chemical and bioactivity. Finally, the *in vitro* antioxidant activity of the studied compound was monitored *via* two radical scavenging inhibitors.

Keywords: Ru(II) nitrosyl complex, FMOs, NLO, Antioxidant activity, ADME.

INTRODUCTION

Nitric oxide (NO$^\bullet$) is a highly reacting radical naturally formed by nitric oxide synthase (NOS), which plays a crucial role in various physiological processes such as blood regulation, neurotransmission, immune response, respiration and cytotoxic activity in tumour cells by apoptosis [1-3]. One area of intense investigation has been the reaction of NO at metal canters in several enzymes. Studies of NO reactivity with metal complexes have yielded important information about metal-NO chemistry. They have resulted in the metal-based NO-sensors and NO-scavenger technologies [4-7]. More recently, transition metal-NO complexes have been developed that act as NO donors by releasing coordinated NO upon exposure to light, which is of significant interest in the medical industry [8-10].

Ruthenium(II/III) complexes have unique and applied features. They are hexa-coordinated in said oxidation states, low spin and their substitution reaction rates are slighter than those of corresponding first row complexes. Ruthenium(II) can back-bonding [11,12], a milestone in coordination chemistry that led to a photochemistry and supramolecular chemistry; also, some of their complexes can iron mimic, a significant feature for biological characteristics [13]. The interaction of metal complexes with NO and metal nitrosyl complexes is crucial for synthesizing new NO donors and for NO scavenging activity [14,15]. Ruthenium complexes belong to an upcoming class of antitumour agents. Numerous unique ruthenium(II/III) complexes also exhibited the anticancer activity [16].

In absence of X-ray details in the current research outputs, molecular characterization is supported by computational investigations is considered for fruitful validation. Among DFT approaches is a robust theoretical technique to validate experimental evaluations [17]. Theoretical studies are essential to elucidate the fundamental properties and communicating extensive information about the physical and chemical properties of the compound. Density functional theory (DFT) in the computational chemistry has been established to apply chemical and biological science research. It has been used to predict and develop structural properties, vibrational spectral, and other spectral characterization of the micro and macro-molecules [18-24]. Molecular orbitals and the simulated electronic absorption spectrum may also be determined by the

TD-DFT method implemented in the Gaussian 09 program [25].

The wide applications computational approaches for this significant class of studies, DFT aspects of ruthenium complexes and eminent seek of diversified properties in terms of both experimental as well as a theoretical asset of nitrosyls complexes, systematic density functionalized studies of newly synthesized Ru(II) nitrosyl complex of *N*-dehydroacetic acid sulfadiazine have been designed. In this study, a comparison of the compound's experimental and theoretical results was carried out using DFT computation methods. The molecular structural framework, frequency calculation and the possible electronic excitations *via* the TD-DFT formalism. Moreover, electrochemistry based HOMO-LUMO and the energy gap (E_g) are calculated. Improved understanding of the compound's nature resulted from an investigation of the experimental, theoretical and *in silico* ADME properties and antioxidant activities of the present compound of interest.

EXPERIMENTAL

Reagents and solvents employed in this work were used as received from commercial suppliers of analytical grade. The electrochemical analysis reveals the redox properties of *cis*-[$RuCl_2(PPh_3)(NO)$(dha-sdz)]. The measurements were carried out on a glassy carbon electrode in DMSO solutions containing 0.1 M tetrabutylammonium tetrafluoroborate (TBATFB) as the supporting electrolyte using a three-electrode cell and BASi Epsilon workstation. Electronic absorption spectra were documented on Carry 5000 UV-Vis/NIR spectrophotometer. The vibrational frequencies were recorded with an αT Bruker FT-IR spectrophotometer from 4000-400 cm^{-1} using the KBr disc method. ^{1}H-chemical shifts δ (ppm) was obtained using Bruker Avance 400/AbIII HD-300 (FT-NMR) and the electron spray ionization spectrogram (ESI-Mass) was recorded at 70 eV between a mass range of 100-1000 at Waters UPLC-TQD Mass spectrometer from CDRI, Lucknow, India. Molar conductance was measured in 10^{-3} M DMF solution at ambient temperature over the digital reading conductivity meter (EUTECH model CON2700). The molar conductance of the studied complex compound is 11.3 Ω^{-1} cm^2 mol^{-1}.

Synthesis of metal precursor [$RuCl_2(NO)(PPh_3)_3$]: The metal precursor, [$RuCl_2(NO)(PPh_3)_3$], was synthesized by the binary step method. In the first step method, the compound [$RuCl_2(PPh_3)_4$] was synthesized by a reported procedure of Stephenson & Wilkinson [26]. $RuCl_3 \cdot 3H_2O$ (200 mg) with six-fold excess of triphenyl phosphene (1200 mg) in methanol. The reaction mixture shaking the solution was filtered. The deep brown solution was shaken at room temperature under nitrogen atmosphere for 24 h. The dark brown crystals were washed with methanol, and diethyl ether, then dry in vacuumed for several hours. In the second step, a solution of [$RuCl_2(PPh_3)_4$] in DCM was bubbled with NO gas about 30 min generated by allowing 30% of HNO_3 to react with copper turning the solution turn to red from brown then kept at room temperature for overnight the desired compound was precipitated.

Synthesis of Schiff base ligand (Hdha-sdz): The sulfa drug derived Schiff base ligand **Hdha-sdz** was synthesized by condensing equimolar quantities of dehydroacetic acid (336 mg, 2 mmol) with sulfadiazine (500 mg, 2 mmol). The reaction mixture was refluxed with constant stirring in ethanol for about 6 h. The desired compound was precipitated as brown mass and filtered off, washed and recrystallized from ethanol. Yield: 1.56 g (75%); *m.w.*: 400, decomposition temperature: 210 ºC. Anal. calcd. (found) % for $C_{18}H_{16}N_4O_5S$: C, 52.65 (53.99); H, 4.00 (4.03); N, 13.85 (13.99. IR (KBr, ν_{max}, cm^{-1}): 3427 (OH), 3362 (NH), 1643 (CO), 1587 (CN) and 1267 (OSO).

Synthesis of *cis*-[$RuCl_2(PPh_3)(NO)$(dha-sdz)] (1): Compound **1** was synthesized with the equimolar quantities of [$RuCl_2(NO)(PPh_3)_3$] (495 mg, 0.5 mmol) with Hdha-sdz (200 mg, 0.5 mmol). The reaction mixture was refluxed with constant stirring in ethanol for about 6 h. The greenish-brown product was precipitated and filtered off, washed with ethanol, and recrystallized from ethanol. Yield: 65%; *m.w.*: 863. decomposition temperature: 260 ºC. Anal. calcd. (found) % $C_{36}H_{30}Cl_2N_5O_6PSRu$: C, 50.00 (50.06); H, 3.39 (3.50); N, 8.09 (8.11). IR (KBr, ν_{max}, cm^{-1}): 3427 (OH), 3362 (NH), 1643 (CO), 1587 (CN)and 1267 (NO).

Antioxidant activity: The antioxidant activity of the title compounds was carried out by two free radical scavenging (FRS) assays *viz.* 1,1-diphenyl-2-picrylhydrazide (DPPH) and nitric oxide radical ($NO^{\bullet}$) are extensive applications. The $DPPH^{\bullet}$ activity was performed with the previously reported procedure by Li *et al*. [27]. According to this procedure, 2 mL of 4% solution of DPPH radical in methanol (w/v) was mixed with 500 µL of sample solutions at various increasing concentrations of 20, 40, 60, 80 and 100 µM. The absorbance was recorded via UV-visible spectrophotometer at 517 nm after half-hour of incubation period of the reaction within the dark compared with the absorbance of control prepared similarly without adding the compounds. The absorbance was decreased with increasing concentration. The lower absorbance indicates a better free radical scavenging activity of the reaction mixture.

Another method is nitric oxide radicals $NO^{\bullet}$ scavenging assay was performed using a slightly modified procedures [28,29]. This activity was monitored in the same concentrations (20-100 µg/mL), The samples were prepared in DMSO and homogeneous solutions were obtained by stirring. The $NO^{\bullet}$ were generated from the mixture of 1mL of sodium nitroprusside (10 mM) and 1.5 mL of phosphate buffer saline (0.2 M, pH 7.4) were added to the test compounds and incubated for ~150 min at 25 ºC. The reaction mixture of above samples (1 mL each) was treated with 1 mL of Griess reagent (1% sulphanilamide, 2% H_3PO_4 and 0.1% naphthylene diamine dihydrochloride). The absorbance was measured at 546 nm using a UV-visible spectrophotometer.

Accordingly, to the above-described assay, all the tests were performed in a triplically. Various said concentrations of Schiff base **Hdha-sdz** and compound **1** were used with the fix concentration at which the compound showed around 50% of scavenging activity. In addition, the percentage of scavenging activity was calculated using the following formula:

$$\text{Scavenging activity } (\%) = \frac{A_o - A_c}{A_o} \times 100$$

where A_o and A_c are the absorbances in absence and presence of the studied compounds, respectively. Thus 50% of scavenging activity (IC_{50}) can be calculated using the percentage of scavenging activity results. Butylated hydroxytoluene (BHT) was used as a standard for both assays.

Theoretical calculations: All the theoretical calculations of the studied compounds were computed *via* the Gaussian 09 programme package [25] using B3LYP/6-31G(dp) and LAN2DZ basis sets using density functional theory (DFT) approaches. The geometry optimization of the compounds produced none of the imaginary frequencies on the computed vibrational spectra confirms that the shape assumed corresponds to minima on their potential energy surface. The computed frequencies and their assignments are aided by using the animation choice of the GAUSSVIEW 5.0 application, which gives a visual presentation of the vibrational modes [30]. In addition, ^{1}H NMR spectra were calculated using the GIAO method and TMS became used as reference material to calculate the chemical shift values [31]. Moreover, the TD-DFT approach [32] has become employed to compute the electronic absorption spectra of the compounds using the solvent effect simulation in DMSO solvent using polarisable continuum model (PCM).

***in silico* ADME properties:** To evaluate the *in silico* ADME properties, is performed to investigate whether the synthesized compounds produce any toxicity after administration in the body or show any pharmacokinetic profile. Proceeding with this purpose, Swiss ADME servers were used.

RESULTS AND DISCUSSION

Sulfa drug-derived Schiff base ligand, *N*-dehydroacetic acid-sulfadiazine (**Hdha-sdz**) and its complex *cis*-[$RuCl_2(PPh_3)$-(NO)(dha-sdz)] **1** were synthesized according to the synthetic route given in **Scheme-I.**

Infrared studies: The experimental and theoretical vibrational spectra of the studied compounds **Hdha-sdz** and *cis*-[$RuCl_2(PPh_3)(NO)$(dha-sdz)] **1** are presented in Figs. 1 and 2, respectively. The observed bands provide a significant explanation for the metal-ligand bonding. The free ligand shows two characteristic peaks at 3426 and 1643 cm^{-1}, assigned the stretching vibrations of ν(OH) and ν(-C=N). After the complexation, the first peak of ν(OH) disappeared from the complex compound. Still, in this region, a new strong peak arises at ~ 3400 cm^{-1} assigned as ν(H_2O) for the moisture or lattice water molecule. The second peak of amine ν(-C=N) is shifted in the lower frequency at 1630 cm^{-1}, suggesting the azomethine nitrogen in coordination. Furthermore, a strong band was observed at 1872 cm^{-1} for coordinated terminal nitrosyl and observed slightly higher frequency than the precursor complexes. Finally, the few other functional groups that display vibrations at 3381 ν(NH), 1326 ν(C-O), 1268 and 1155 are attributed as asymmetric and symmetric stretching of ν(O=S=O), 568 ν(Ru-NO), 521 ν(Ru-O) and 456 ν(Ru-Cl). The DFT-based theoretical vibrational IR spectra of the title compounds were computed with Gaussian 09 program. The animation program of Gauss View 05 was used to enlighten the functional group assignments. The experimental and theoretical frequencies show a remarkable resemblance to each other. Some slight differences in the values wavenumber might be due to the polarization effect, computation scheme and experimental conditions.

^{1}H NMR studies: The experimental and theoretical ^{1}H NMR spectrum of *cis*-[$RuCl_2(PPh_3)(NO)$(dha-sdz)] (**1**) is shown in Fig. 3. The experimental ^{1}H NMR spectrum was recorded

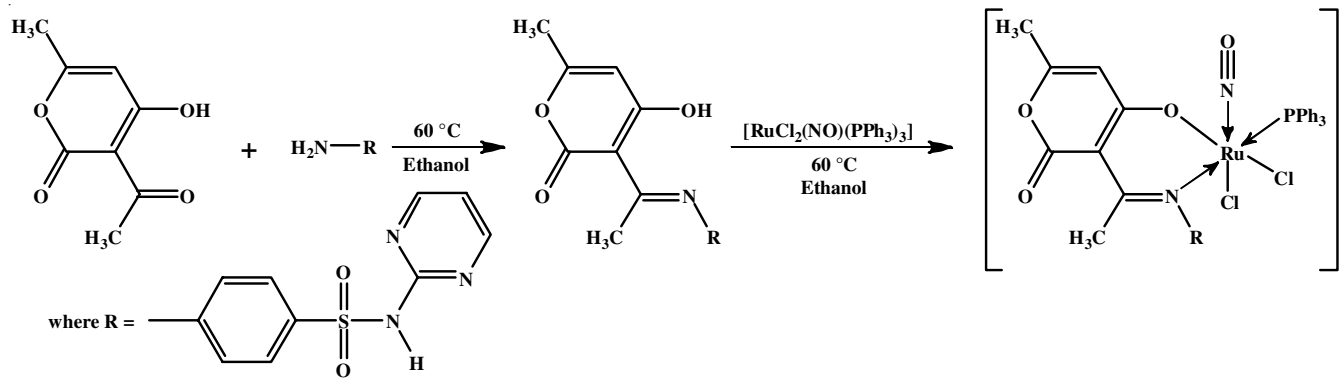

Scheme-I: Synthetic route of Schiff base ligand **Hdha-sdz** and its Ru(III) complex **1**

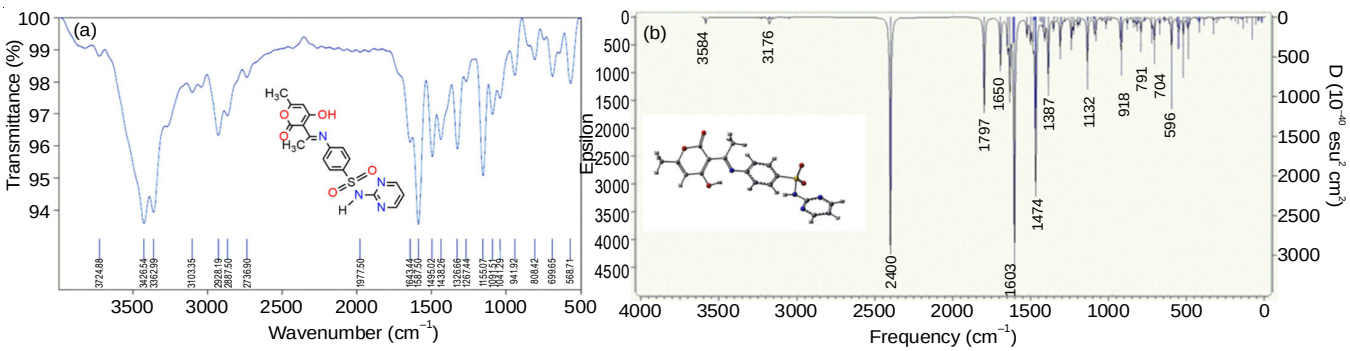

Fig. 1. Experimental and theoretical infrared spectrum of **Hdha-sdz**

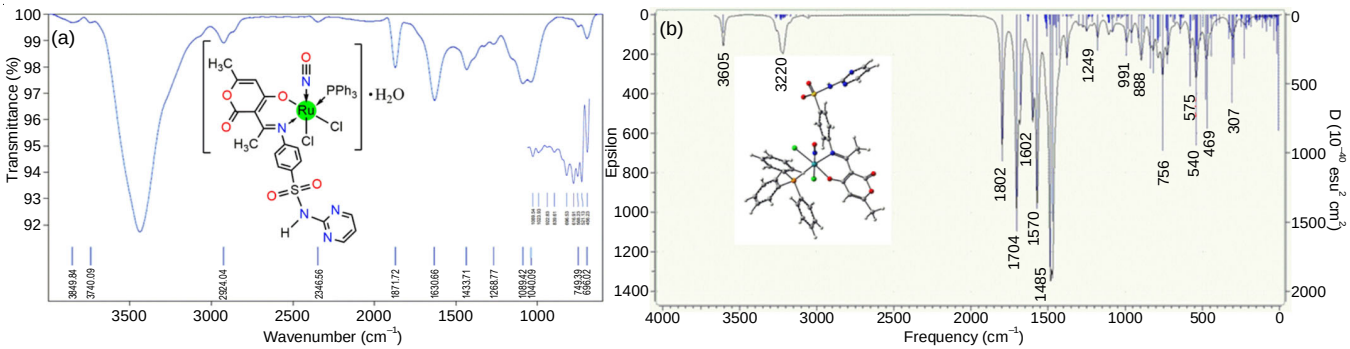

Fig. 2. Experimental and theoretical infrared spectrum of compound **1**

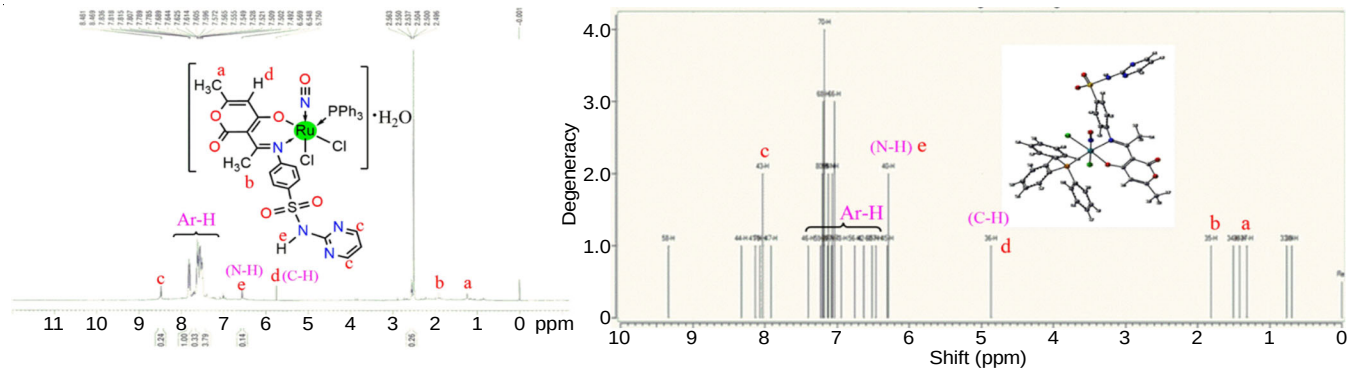

Fig. 3. Experimental and theoretical ^{1}H NMR spectrum of compound **1**

using a DMSO-d_6 environment at room temperature. While, the theoretical ^{1}H-chemical shifts δ (ppm) was computed with the gauge independent atomic orbital (GIAO) method and tetramethylsilane (TMS) was used as reference material with the DFT approach. The theoretical ^{1}H-chemical shifts δ (ppm) data is given in parenthesis. The singlet peak found at 5.7 (4.9) ppm has been assigned to the vinylic proton of the pyrone ring of the dehydroacetic moiety. A single peak at 6.5 (6.3) ppm have been attributed to the -NH proton of sulfadiazine moiety of the Schiff base ligand. The multiple peaks were observed in the region 7.0-7.9 (6.7-7.5) ppm are assigned as aromatic ring protons. The singlet signals are having been observed at 1.3 (1.4) and 1.9 (1.8) ppm due to three protons of CH_3-C(a) and CH_3-C=N(b), respectively. The singlet peak was observed at 8.4 (8.2) ppm due to a single proton of H-C=N(c). The appearance of two singlets around 2.8 ppm can be assigned to the presence of DMSO as solvent. The theoretical spectrum shows a remarkable similarity to the experimental vibrational spectral data. Some variance in the values of experimental and theoretical chemical shifts might be due to the polarization, scheme of computation and experimental conditions.

Electronic spectrum: The experimental and theoretical UV-visible transitional absorption spectrum of compound **1** is shown in Fig. 4 and the data is presented in Table-1. The electronic absorption spectrum of 10^{-5} M of both studies Schiff base **Hdha-sdz** and compound **1** was recorded in DMSO. While the theoretical spectrum was computed using the PCM model using the time-dependent density functional theory (TD-DFT) method. The experimental λ_{max} was observed three excitations at 276, 313 and 410 nm. In contrast, the theoretical spectrum was also found three excitations at 331 nm between HOMO-1 to LUMO, 393 nm HOMO to LUMO+1 and 403 nm HOMO to LUMO. The coordinated organic framework is apparent and the modest rise in absorption near-visible range assigns

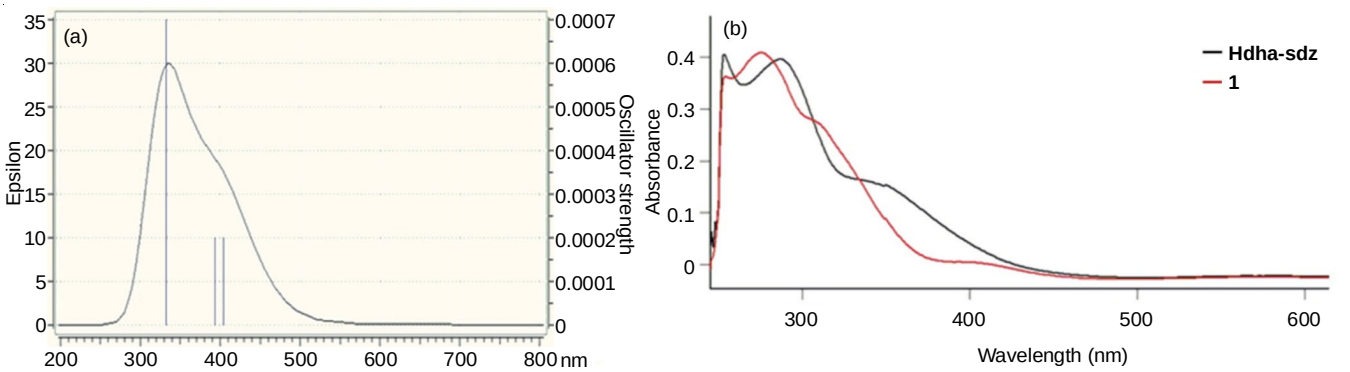

Fig. 4. Theoretical (a) and experimental (b) electronic spectrum of compound **1**

TABLE-1
OBSERVED AND COMPUTED ELECTRONIC ABSORPTION SPECTRAL DATA AND SIGNIFICANT ORBITAL CONTRIBUTION WITH OSCILLATOR STRENGTH OF COMPOUND *cis*-[$RuCl_2(PPh_3)(NO)$(dha-sdz)] (**1**)

λ_{max} (nm)		eV	Oscillator strength (*f*)	Major contribution (%)	Peak assignment
Obs.	Comp.				
276	331	3.746	0.0007	H-1(α) → L(α)(45%)	ILCT
313	393	3.155	0.0002	H(α)→ L+1(α)(60%)	LMCT
410	403	3.077	0.0002	H(α)→ L(α)(62%)	MLCT

HOMO (H), LUMO (L), Intra ligand charge transfer transition (ILCT), Ligand to metal charge transfer transition (LMCT) and Metal to ligand charge transfer transition (LMCT).

the nitrosyl ligand photo lability. The discussion appears to have been successful in depopulating HOMO and populating LUMO to carry out a bonding M-NO as well as and an anti-bonding M-NO character, respectively, resulting in the NO's release. A total of 537 molecular orbitals involves in the electron density distributions and electronic excitations. While the orbital number 185 is meant for HOMO and 186 for LUMO. The energy gap of HOMO and LUMO is 2.994 eV. FMOs involve in electronic transition observed in TD-DFT computed UV-vis spectrum of compound **1** (Fig. 5).

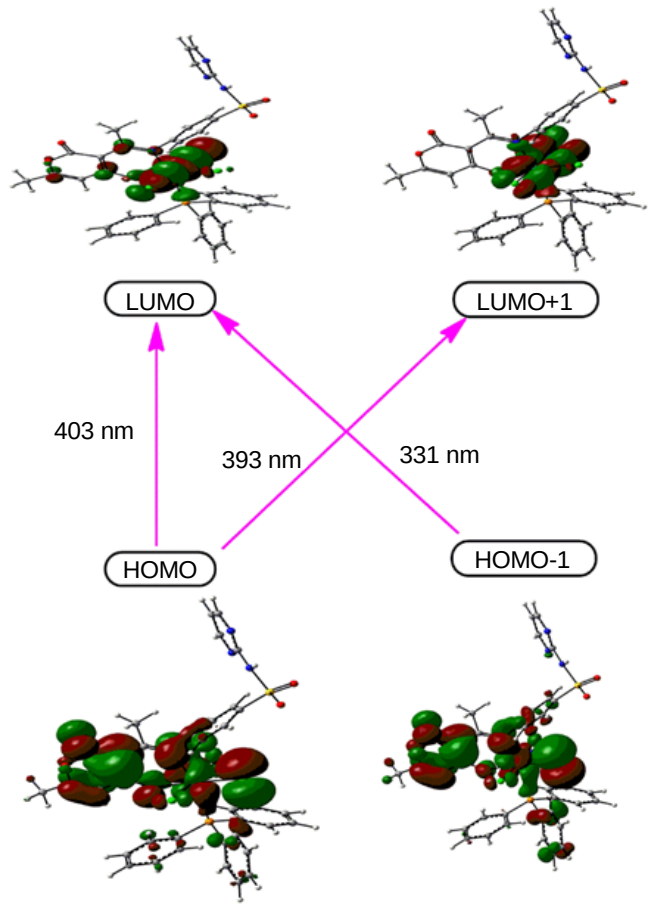

Fig. 5. FMOs involve in electronic transition observed in TD-DFT computed UV-vis spectrum of compound **1**

Cyclic voltammetry: The electrochemical properties of compound **1** were monitored. The voltammogram (Fig. 6) shows the two-step irreversible reduction wave E_{pc1} (0.156) and E_{pc2} (-0.557) in V and I_{pc1} (-0.872) and I_{pc1} (-2.052) μA that can be

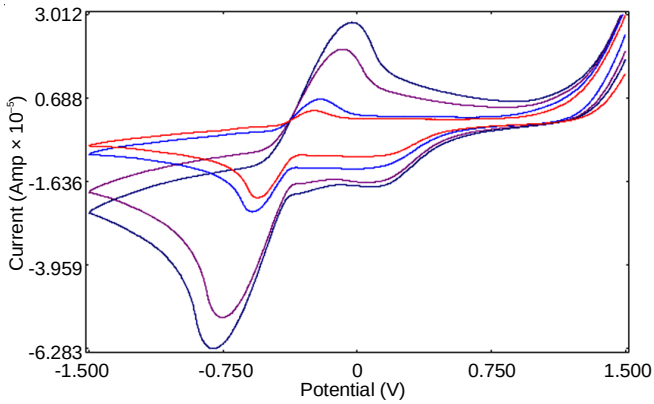

Fig. 6. Cyclovoltammetry curve of compound **1**

used to establish $Ru\text{-}NO^+ \rightarrow Ru\text{-}NO^0$ and $Ru\text{-}NO^0 \rightarrow Ru\text{-}NO^-$ components. The voltammogram also shows a single step irreversible oxidation wave E_{pa1} (-0.237) V and I_{pa1} (0.307) μA that can be used to establish and $Ru\text{-}NO^- \rightarrow Ru\text{-}NO^0$ component. The compound under goes quasi reversible redox behaviour. Such electron shifting studies may also be associated with frontier molecular orbitals analyses that significantly impact formulating chemical descriptors [33]. The value of HOMO and LUMO levels and its energy gap (E_g) were calculated from the E_{ox} (onset) potential of electrochemical reduction and oxidation which are tabulated in Table-2. The experimental HOMO and LUMO approximation were made with the help of cyclic voltammograms, empirical relation $E_{HOMO} = [(E_{ox} - E_{1/2(ferrocene)} + 4.8]$ eV. Ferrocene was used as standard. $E_{1/2(ferrocene)}$ is equal to 0.304 V, which can be used to calculate E_{HOMO}. We can calculate the band gap (E_g) in eV from the electronic absorption spectra 1242/λ (nm). Meanwhile, Schiff base **Hdha-sdz** and compound **1** lead the HOMO; their HOMO energy levels are similar with slight variation. The value of E_{LUMO} and $E_{HOMO} - E_{LUMO}$ of compound **1** is shown in Table-3. While theoretical energy gap (ΔE) was calculated from TD-DFT approaches, the energy gap between HOMO and LUMO is 3.13 eV. Thus, one can determine the way the molecule interacts with other species. Hence, they are called the frontier orbitals. The HOMO is the molecular orbital that mainly acts as an electron donor. The LUMO is the orbital that mainly assists as the electron acceptor. The energy gap between HOMOs and LUMOs characterises the molecular chemical stability [34,35].

Antioxidant properties: The antioxidant activity of both Schiff base **Hdha-sdz** and compound **1** was assessed *in vitro* using DPPH and NO radical scavenging techniques. The activity of the investigated substances was measured at five different

TABLE-2
ELECTROCHEMICAL DATA OF COMPOUND *cis*-[$RuCl_2(PPh_3)(NO)$(dha-sdz)] (**1**)

Scan rate (mV s^{-1})	E_{pc1} (V)	I_{pc1} (μA)	E_{pc2} (V)	I_{pc2} (μA)	E_{pa1} (V)	I_{pa1} (μA)	E_r (V)	ΔE (V)	I_{pa}/I_{pc}
100	0.156	-0.872	-0.557	-2.052	-0.237	0.307	-0.397	0.320	0.150
200	0.066	-1.218	-0.582	-2.455	-0.204	0.681	-0.393	0.378	0.277
300	0.041	-1.621	-0.754	-5.390	-0.090	2.062	-0.422	0.664	0.383
500	0.066	-1.793	-0.803	-6.283	-0.041	2.781	-0.422	0.762	0.443

Tetrabutylammonium perchlorate (0.1 M); concentration of complex, 0.001 M; all the potentials are referenced to Ag/AgCl electrode; $E_r = 0.5 (E_{pa} + E_{pc})$, where E_{pa} and E_{pc} are anodic and cathodic potentials.

TABLE-3
HOMO-LUMO VALUES FROM ELECTROCHEMICAL AND ELECTRONIC ABSORPTION SPECTROSCOPIC DATA

Compound	E_{ox} V (from CV)	E_{HOMO} eV [E_{ox}-$E_{1/2}$ + 4.8]	Optical band gap from absorption studies (eV) 1242/λ (nm)	E_{LUMO} (E_{HOMO}-optical band gap)	$E_{HOMO-LUMO}$
Hdha-sdz	0.154	4.65	4.58	0.07	4.58
1	-0.237	4.26	4.30	-0.041	4.30

concentrations (20, 40, 60, 80 and 100 μg/mL) with butylated hydroxyl toluene (BHT) serving as a standard for comparison. The *in-vitro* antioxidant activities of compound **1** is observed about 61.78 ± 2.0 μM and 70.61±1.8 μM for $DPPH^{\bullet}$ and $NO^{\bullet}$ scavenging assays, respectively. While Schiff base **Hdha-sdz** has not resulted antioxidant activity at this concentration.

Molecular structure framework: Fig. 7 shows the evolution of optimized molecular modelling frameworks of the examined compounds **Hdha-sdz** and *cis*-[$RuCl_2(PPh_3)$-(NO)(dha-sdz)] (**1**). Table-4 shows the specified geometrical properties, such as required bond length (Å) and bond angles (º). Compound **1** has a somewhat deformed octahedral geometry with six coordinates around the Ru(II) centre, which correspond to O, 2Cl, 2N and P. The angle of atoms confirms the slight deviation of this octahedral geometry in three transpositions, which is different from 180° [$O_{(11)}$-Ru-$Cl_{(48)}$, 175.292°; $N_{(12)}$-Ru-$P_{(82)}$, 171.252° and $Cl_{(30)}$-Ru-$N_{(31)}$, 177.599°]. The basal plane comprises four donor atoms like O and N atoms of the monobasic bidentate ligand and two monodentate ligands like one Cl and one P atom. A sulfa drug Schiff base ligand binds with the ruthenium atom as monobasic bidentate ON donor atoms forming one six-membered chelate rings RuO11C6-C3C2N12 with a bite angle of $O_{(11)}$-Ru-$N_{(12)}$ 87.614. The two-chlorine atoms are in *a cis* position to $Cl_{(30)}$-Ru-$Cl_{(48)}$, 90.936º, and the nitrosyl lie *trans* to chlorine. The distance of Ru-Cl (30) 2.425 Å is shorter than the bond length of another chlorine atom present in the same molecule, Ru–Cl (48) 2.484 Å. This is expected due to the trans strengthening effect of the NO group [36,37]. The interatomic distance of N-O is close to 1.193 Å; the same length in the free NO^+ 1.06 is shorter, showing the absence of back boning. While the atomic distance of Ru-NO is 1.763 Å is shorter due to the π back bonding effect of the nitrosyl ligand. The Ru–P has a bond length of 2.537 Å, which is comparable to that of other ruthenium complexes. In these cases, the chlorine atom is trans to the phosphene (Cl-Ru-P), and the bond distance is 2.484 Å due to the trans effect. In ligand, the (-C=N-) and (C–O) distance observed are 1.341 and 1.263 Å, while, after the complexation, the bond distances between said atoms are observed 1.334 and 1.316 Å are increased due to lone pair of electrons moving from ligand to metal site.

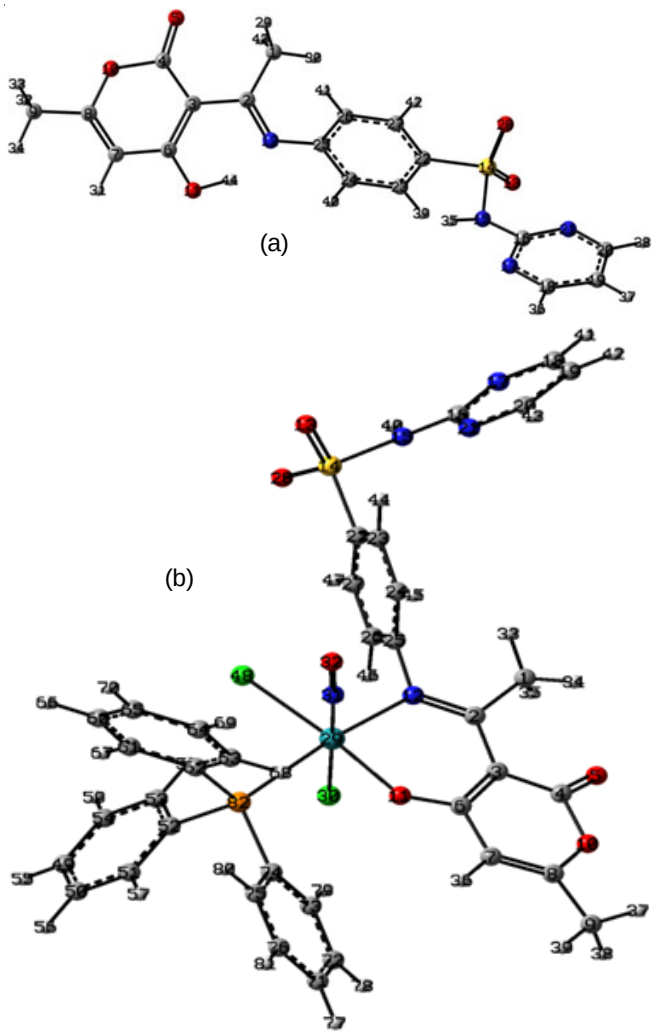

Fig. 7. Computed optimized molecular structure of **Hdha-sdz** (a) and **1** (b) obtained *via* B3LYP/6-31G*(dp)/LANL2DZ level with numbering scheme

NLO Assets: The non-linear optical (NLO) properties of organic and inorganic materials are receiving a lot of interest. Because of their potential applications for optical telecommunication, optical data storage, optical interconnects, integrated optics signal processing and image modernization technologies

TABLE-4
SELECTED GEOMETRICAL AND PARAMETERS OF COMPOUND **1**

Bond connectivity	(Å)	Bond connectivity	(°)	Parameters	**Hdha-sdz**	**1**
$Ru\text{-}O_{(11)}$	2.046	$O_{(11)}\text{-}Ru\text{-}N_{(12)}$	87.614	η	-2.177	-1.497
$Ru\text{-}N_{(12)}$	2.127	$O_{(11)}\text{-}Ru\text{-}Cl_{(30)}$	87.752	χ_{abs}	-4.572	-5.116
$Ru\text{-}Cl_{(30)}$	2.425	$O_{(11)}\text{-}Ru\text{-}N_{(31)}$	94.466	μ	6.399 D	11.663D
$Ru\text{-}N_{(31)}$	1.763	$O_{(11)}\text{-}Ru\text{-}Cl_{(48)}$	175.292	HOMO	-6.749	-6.613
$Ru\text{-}Cl_{(48)}$	2.484	$O_{(11)}\text{-}Ru\text{-}P_{(82)}$	89.141	HOMO-1	-7.021	-6.776
$Ru\text{-}P_{(82)}$	2.537	$N_{(12)}\text{-}Ru\text{-}Cl_{(30)}$	85.186	HOMO-2	-7.266	-6.912
$N_{(31)}\text{-}O_{(32)}$	1.193	$N_{(12)}\text{-}Ru\text{-}N_{(31)}$	93.978	LUMO	-2.395	-3.619
$N_{(12)}\text{-}C_{(2)}$	1.334	$N_{(12)}\text{-}Ru\text{-}Cl_{(48)}$	96.784	LUMO+1	-1.578	-3.592
$O_{(11)}\text{-}C_{(6)}$	1.316	$N_{(12)}\text{-}Ru\text{-}P_{(82)}$	171.252	LUMO+2	-1.551	-2.395
		$Cl_{(30)}\text{-}Ru\text{-}N_{(31)}$	177.599	$\Delta E_{HOMO-LUMO}$	4.354	2.994
		$Cl_{(30)}\text{-}Ru\text{-}Cl_{(48)}$	90.936	$\Delta E_{HOMO-1-LUMO+1}$	5.443	3.184
		$Cl_{(30)}\text{-}Ru\text{-}P_{(82)}$	86.571	$\Delta E_{HOMO-2-LUMO+2}$	5. 715	4.517
		$N_{(31)}\text{-}Ru\text{-}Cl_{(48)}$	86.924			
		$N_{(31)}\text{-}Ru\text{-}P_{(82)}$	94.372			
		$Cl_{(48)}\text{-}Ru\text{-}P_{(82)}$	86.267			
		$Ru\text{-}N_{(31)}\text{-}O_{(32)}$	174.916			

Absolute hardness (η); Absolute electronegativity (χ_{abs}) dipole moment (μ)

[38,39]. Theoretical chemistry executes an essential character to understanding the structural assets connection, which could assist the design of novel NLO materials. It is confirmed that the compound has the largest values of dipole moment (μ), polarizability (α), anisotropy of the polarizability ($\Delta\alpha$) and first static calculated hyperpolarizability (β_o) are suitable NLO active materials. Hence, the NLO properties were theoretically calculated based on the relationship of x, y, z components [40]. The finite field approach calculates this novel molecular system's first hyperpolarizability (β_o) by the DFT technique. It is a third rank tensor [3 × 3 × 3] matrices can describe. The Kleinman symmetry [41] allows the twenty-seven components of the 3D matrix to be reduced to ten components. In connection with herein calculated the NLO properties of the studied Schiff base **Hdha-sdz** and compound **1**. The computed values concerning their tensor orders are summarized in Table-5. The values in the order are 6.399 D, -160.256×10^{-24}, 43.913×10^{-24}, and 345.864×10^{-31} esu for **Hdha-sdz** 11.663D, -323.296×10^{-24}, 56.277×10^{-24} and 551.407×10^{-31} esu for complex **1**. The polarizabilities and first-order hyperpolarizabilities are expressed in the atomic units (au), the calculated values have been converted into electrostatic units (esu) through the conversion factor of 0.148×10^{-24} esu for α and 8.639×10^{-33} esu for β. Urea is one of the model compounds used as NLO active material. Because there were no experimental measurements of NLO characteristics of the examined compounds, urea was chosen as a reference in this investigation. One of the most important aspects of the NLO system is the extent of molecule hyperpolarizability. Generally speaking, highly efficient NLO materials have notable charge transfer (CT) transitions.

TABALE-5
DIPOLE MOMENT (μ), POLARIZABILITY (α), ANISOTROPY OF THE POLARIZABILITY ($\Delta\alpha$) AND HYPERPOLARIZABILITY (β)

	Hdha-sdz	Compd. **1**
μ_x	-3.049	8.103
μ_y	-5.593	4.999
μ_z	0.608	6.736
$\mu_{Tot.}$	6.399	11.663
α_{xx}	-131.474	-289.136
α_{yy}	-179.375	-353.812
α_{zz}	-169.828	-326.940
α_{xy}	1.213	-35.157
α_{xz}	12.730	-8.642
α_{yz}	-1.929	13.757
α	-160.256×10^{-24}	-323.296×10^{-24}
$\Delta\alpha$	43.913×10^{-24}	56.277×10^{-24}
β_{xxx}	60.017	33.871
β_{yyy}	-17.821	-32.081
β_{zzz}	1.770	48.974
β_{xyy}	-6.311	310.471
β_{xxy}	-323.409	357.996
β_{xxz}	7.290	159.107
β_{xzz}	-24.496	31.269
β_{yzz}	-3.224	-49.003
β_{yyz}	1.904	85.663
β_{xyz}	9.441	-27.243
$\beta(0)$	345.864×10^{-31}	551.407×10^{-31}

Molecular electrostatic potentials: MEP map predicts molecule reactivity, permits visualization of variable potential regions inside molecules and gives transparent charge distribution information. The MEP of molecules is governed by electron distribution. Different colours depict different values of the electrostatic potential at the surface. The electrophilicity and nucleophilicity of the compounds are related to the potential, which increases from negative to positive charges in the order of red < orange < yellow < green < blue. As shown in the MEP map, the largest negative potentials region correlates to the most electronegative atoms (Fig. 8). The maximum negative potentials region corresponds to the most electronegative atoms.

In contrast, the leading positive area corresponds to the greatest electropositive atoms. Herein, the oxygen atoms of the sulfa drug moiety are more electronegative. At the same time, the maximum positive region is localised on hydrogen atoms, which correspond to the neutral groups. The remaining species are surrounded by zero potential.

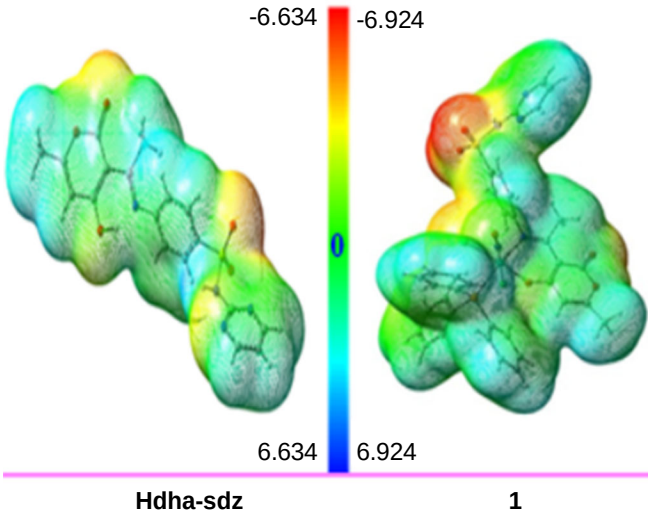

Fig. 8. 3D MESP surface map of Schiff base **Hdha-sdz** (left) and compound **1** (right)

***in silico* ADME studies:** *In silico* ADME properties were studied through the Swiss ADME predictor (http://www.swissadme.ch), which shows the biological potential and oral administrative activity of the compound. The Swiss ADME predictor provides more applicable information about the compounds such as molecular hydrophobicity (log P), topological polar surface area (TPSA) and bioavailability. According to Lipinski' rule, the log P values are observed to be less than five, indicating a higher tendency to ease penetration to the cell membrane. To be analyzed by hydrogen bondability in the system, which is used to predict drug transport properties inside various body parts such as gastrointestinal tract, bioavailability, blood-brain barrier penetration. The metabolism is expected based on five cytochrome phosphate (CYP) models (CYP1A2, CYP2C19, CYP2C9, CYP2D6 and CYP3A4) inhibitors and one phosphatase glycoprotein (P-gp) substrate. These parameters were computed and verified for compliance with their standard ranges.

Herein, we examined the *in silico* ADME properties of compounds **Hdha-sdz** and *cis*-[$RuCl_2(PPh_3)(NO)$(dha-sdz)] (**1**). Schiff base **Hdha-sdz** contains two hydrogen bond donors (HBD), eight hydrogen bond acceptors (HBA) and five rotatable bonds. While compound **1** hold one H-bond donor and nine H-bond acceptors with eight rotatable bonds, divulging that they are active in the oral mode of administration. The TPSA values of **Hdha-sdz** and compound **1** are 143.13 and 169.51 $Å^2$, respectively. According to Veber's and Lipinski' rules, if the number of rotatable bonds in the system is ~10, it supports the oral bioavailability of the compounds (Table-6). The bioavailability score of **Hdha-sdz** and compound **1** are 0.55 and 0.17, respectively. Therefore, the bioavailability score is achieving more than zero. They possess a higher probability and investigated compounds' good biological activity increases. If the solubility score log S is defined in the order of < -10; insoluble, < -6; poorly soluble, < -4; moderate soluble, < -2; soluble and < 0; highly soluble. In the current study, the ligand is -3.34; it is soluble while the complex is -9.74 is poorly soluble.

TABLE-6
In silico ADME PROPERTIES OF STUDIED COMPOUNDS **Hdha-sdz** AND COMPOUND **1**

	Hdha-sdz	Compd. **1**
Physico-chemical parameters		
Formula	$C_{18}H_{16}N_4O_5S$	$C_{36}H_{30}N_5O_6PRuSCl_2$
Molecular weight	400.41 g/mol	863.67 g/mol
Num. heavy atoms	28	52
Num. arom. heavy atoms	18	36
Fraction Csp3	0.11	0.06
No. rotatable bonds	5	8
No. H-bond acceptors	8	9
No. H-bond donors	2	1
Molar Refractivity	103.17	204.37
TPSA	143.13 Å²	169.51 Å²
log S (solubility)	-3.34	-9.74
Pharmacokinetic parameters		
GI absorption	Low	Low
BBB permeant	No	No
P-gp substrate	No	No
CYP1A2 inhibitor	No	Yes
CYP2C19 inhibitor	No	No
CYP2C9 inhibitor	Yes	No
CYP2D6 inhibitor	No	No
CYP3A4 inhibitor	Yes	Yes
log K_n (skin permeation)	-7.76 cm/s	-6.43 cm/s
log P (lipophilicity)	1.74	3.84
Bioavailability score	0.55	0.17
Synthetic accessibility	3.65	6.34

Conclusion

The synthesis and the theoretical investigations of *N*-dehydroacetic acid-sulfadiazine ligand (**Hdha-sdz**) and its Ru(III) complex *viz*. *cis*-[$RuCl_2(PPh_3)(NO)$(dha-sdz)] (**1**) are reported. The infrared, chemical shift and electronic absorption spectra were computed and related to experimental results. In addition, computational analyses like FMOs, NLO properties, and MEP surface analyses investigated the studied compounds. The NLO properties were observed through values of dipole moment, polarizability and hyperpolarizability. *In vitro* scavenging activities of compound **1** is observed about 61.78 ± 2.0 μM and 70.61 ± 1.8 μM for $DPPH^•$ and $NO^•$ assays, respectively. The compound **Hdha-sdz** has not resulted at this concentration. The *in silico* ADME results are attributed to good pharmacokinetics and biological activity.

ACKNOWLEDGEMENTS

The authors acknowledge to Prof. Kapil Deo Mishra, Vice-Chancellor, Rani Durgavati Vishwavidyalaya, Jabalpur for their moral support and inspiration. Thanks are also due to The Head, Department of Chemistry for providing instrumentational facilities. In addition, analytical facilities provided by the SAIF, Central Drug Research Institute, Lucknow, India are also acknowledged.

CONFLICT OF INTEREST

The authors declare that there is no conflict of interests regarding the publication of this article.

REFERENCES

1. P. Picón-Pagès, J. Garcia-Buendia and F.J. Muñoz, *Biochim. Biophys. Acta Mol. Basis Dis.*, **1865**, 1949 (2019); https://doi.org/10.1016/j.bbadis.2018.11.007
2. S. Habib and A. Ali, *Indian J. Clin. Biochem.*, **26**, 3 (2011); https://doi.org/10.1007/s12291-011-0108-4
3. S. Singh and A.K. Gupta, *Cancer Chemother. Pharmakoi.*, **67**, 1211 (2011); https://doi.org/10.1007/s00280-011-1654-4
4. T. Nagano and T. Yoshimura, *Chem. Rev.*, **102**, 1235 (2002); https://doi.org/10.1021/cr010152s
5. M.H. Lim and S.J. Lippard, *Acc. Chem. Res.*, **40**, 41 (2007); https://doi.org/10.1021/ar950149t
6. C.J. Marmion, B. Cameron, C. Mulcahy and S.P. Fricker, *Curr. Top. Med. Chem.*, **4**, 1585 (2004); https://doi.org/10.2174/1568026043387322
7. F.G. Marcondes, A.A. Ferro, A. Souza-Torsoni, M. Sumitani, M.J. Clarke, D.W. Franco, E. Tfouni and M.H. Krieger, *Life Sci.*, **70**, 2735 (2002); https://doi.org/10.1016/S0024-3205(02)01528-X
8. M.J. Rose and P.K. Mascharak, *Curr. Opin. Chem. Biol.*, **12**, 238 (2008); https://doi.org/10.1016/j.cbpa.2008.02.009
9. P.C. Ford and I.M. Lorkovic, *Chem. Rev.*, **102**, 993 (2002); https://doi.org/10.1021/cr0000271
10. P.C. Ford, J. Bourassa, K. Miranda, B. Lee, I. Lorkovic, S. Boggs, S. Kudo and L. Laverman, *Coord. Chem. Rev.*, **171**, 185 (1998); https://doi.org/10.1016/S0010-8545(98)90031-5
11. A.D. Allen, F. Bottomley, R.O. Harris, V.P. Reinsalu and C.V. Senoff, *J. Am. Chem. Soc.*, **89**, 5595 (1967); https://doi.org/10.1021/ja00998a016
12. C. Creutz and H. Taube, *J. Am. Chem. Soc.*, **95**, 1086 (1973); https://doi.org/10.1021/ja00785a016
13. D.D. Walker, Ph.D. Dissertation, Stanford University (1980).
14. B.R. Cameron, M.C. Darkes, H. Yee, M. Olsen, S.P. Fricker, R.T. Skerlj, G.J. Bridger, N.A. Davies, M.T. Wilson, D.J. Rose and J. Zubieta, *Inorg. Chem.*, **42**, 1868 (2003); https://doi.org/10.1021/ic020219+
15. S.P. Fricker, *Platin. Met. Rev.*, **39**, 150 (1995).
16. M. Brindell, I. Stawoska, J. Supel, A. Skoczowski, G. Stochel and R. Van Eldik, *J. Biol. Inorg. Chem.*, **13**, 909 (2008); https://doi.org/10.1007/s00775-008-0378-3
17. J.M. Mir, R.C. Maurya and P.K. Vishwakarma, *Karbala Int. J. Modern Sci.*, **3**, 212 (2017); https://doi.org/10.1016/j.kijoms.2017.08.006
18. P.V.R. Rao, K. Srishailam, L. Ravindranath, B.V. Reddy and G.R. Rao, *J. Mol. Struct.*, **1180**, 665 (2019); https://doi.org/10.1016/j.molstruc.2018.12.036
19. M.A. Palafox, V.B. Jothy, S. Singhal, I.H. Joe, S. Kumar and V.K. Rastogi, *Spectrochim. Acta A Mol. Biomol. Spectrosc.*, **116**, 509 (2013); https://doi.org/10.1016/j.saa.2013.07.028
20. S.P. Kollur, J.O. Castro, J. Frau and D. Glossman-Mitnik, *J. Mol. Struct.*, **1180**, 300 (2019); https://doi.org/10.1016/j.molstruc.2018.11.061
21. J.M. Mir, N. Jain, B.A. Malik, R. Chourasia, P.K. Vishwakarma, D.K. Rajak and R.C. Maurya, *Inorg. Chim. Acta*, **467**, 80 (2017); https://doi.org/10.1016/j.ica.2017.07.051
22. K. Murugan, S. Vijayapritha, V. Kavitha and P. Viswanathamurthi, *Polyhedron*, **190**, 114737 (2020); https://doi.org/10.1016/j.poly.2020.114737
23. W. Selmi, N. Hosni, M. Marchivie, H. Maghraoui-Meherzi and M.F. Zid, *J. Mol. Struct.*, **1228**, 129719 (2021); https://doi.org/10.1016/j.molstruc.2020.129719
24. J.M. Mir, P.K. Vishwakarma and R.C. Maurya, *J. Chin. Adv. Mater. Soc.*, **6**, 55 (2018); https://doi.org/10.1080/22243682.2017.1407669
25. M.J. Frisch, G.W. Trucks, H.B. Schlegel, G.E. Scuseria, M.A. Robb, J.R. Cheeseman, G. Scalmani, V. Barone, B. Mennucci, G.A. Petersson, H. Nakatsuji, M. Caricato, X. Li, H.P. Hratchian, A.F. Izmaylov, J. Bloino, G. Zheng, J.L. Sonnenberg, M. Hada, M. Ehara, K. Toyota, R. Fukuda, J. Hasegawa, M. Ishida, T. Nakajima, Y. Honda, O. Kitao, H. Nakai, T. Vreven, J.A. Montgomery Jr., J.E. Peralta, F. Ogliaro, M. Bearpark, J.J. Heyd, E. Brothers, K.N. Kudin, V.N. Staroverov, T. Keith, R. Kobayashi, J. Normand, K. Raghavachari, A. Rendell, J.C. Burant, S.S. Iyengar, J. Tomasi, M. Cossi, N. Rega, J.M. Millam, M. Klene, J.E. Knox, J.B. Cross, V. Bakken, C. Adamo, J. Jaramillo, R. Gomperts, R.E. Stratmann, O. Yazyev, A.J. Austin, R. Cammi, C. Pomelli, J.W. Ochterski, R.L. Martin, K. Morokuma, V.G. Zakrzewski, G.A. Voth, P. Salvador, J.J. Dannenberg, S. Dapprich, A.D. Daniels, O. Farkas, J.B. Foresman, J.V. Ortiz, J. Cioslowski and D.J. Fox, GAUSSIAN 09 (Revision C.01), Gaussian, Inc., Wallingford, CT (2010).
26. T.A. Stephenson and G. Wilkinson, *J. Inorg. Nucl. Chem.*, **28**, 945 (1966); https://doi.org/10.1016/0022-1902(66)80191-4
27. T. Li, S. Li, Y. Dong, R. Zhu and Y. Liu, *Food Chem.*, **145**, 335 (2014); https://doi.org/10.1016/j.foodchem.2013.08.036.
28. L.C. Green, D.A. Wagner, J. Glogowski, P.L. Skipper, J.K.S.R. Wishnok and S.R. Tannenbaum, *Anal. Biochem.*, **126**, 131 (1982); https://doi.org/10.1016/0003-2697(82)90118-X
29. L. Marcocci, J.J. Maguire, M.T. Droy-Lefaix and L. Packer, *Biochem. Biophys. Res. Commun.*, **201**, 748 (1994); https://doi.org/10.1006/bbrc.1994.1764
30. R. Dennington, T. Keith and J. Millam, Gauss View, Version 5, Semichem Inc., Shawnee Mission KS (2009).
31. K. Wolinski, J.F. Hinton and P. Pulay, *J. Am. Chem. Soc.*, **112**, 8251 (1990); https://doi.org/10.1021/ja00179a005
32. K. Burke and E.K.U. Gross, Eds.: D. Joubert, A Guided Tour of Time-Dependent Density Functional Theory in Density Functionals: Theory and Applications, Springer, pp 500 (1998).
33. D. Shoba, S. Periandy, M. Karabacak and S. Ramalingam, *Spectrochim. Acta A*, **83**, 540 (2011); https://doi.org/10.1016/j.saa.2011.09.002
34. S.A. Kumar and B.L. Bhaskar, *IOP Conf. Series Mater. Sci. Eng.*, **310**, 012124 (2018); https://doi.org/10.1088/1757-899X/310/1/012124
35. M.K. Parte, P.K. Vishwakarma, P.S. Jaget and R.C. Maurya, *J. Coord. Chem.*, **74**, 584 (2021); https://doi.org/10.1080/00958972.2021.1880574
36. A.A. Batista, C. Pereira, K. Wohnrath, S.L. Queiroz, R.H. de A. Santos and M.T. do P. Gambardella, *Polyhedron*, **18**, 2079 (1999); https://doi.org/10.1016/S0277-5387(99)00084-4
37. B.L. Haymore and J.A. Ibers, *Inorg. Chem.*, **14**, 3060 (1975); https://doi.org/10.1021/ic50154a041
38. X. Liu, Z. Wang, X. Wang, G. Zhang, S. Xu, A. Duan, S. Zhang, Z. Sun and D. Xu, *Cryst. Growth Des.*, **8**, 2270 (2008); https://doi.org/10.1021/cg7009513
39. P.N. Prasad, *Polymer*, **32**, 1746 (1991); https://doi.org/10.1016/0032-3861(91)90357-O
40. R. Zhang, B. Du, G. Sun and Y. Sun, *Spectrochim. Acta A Mol. Biomol. Spectrosc.*, **75**, 1115 (2010); https://doi.org/10.1016/j.saa.2009.12.067
41. D.A. Kleinman, *Phys. Rev.*, **126**, 1977 (1962); https://doi.org/10.1103/PhysRev.126.1977